Final Technical Report
USGS 06HQGR0151

DYNAMICS OF EPISODIC TREMOR AND SLIP ALONG THE CASCADIA MARGIN

H. Dragert, H. Kao, G.C. Rogers, J. Cassidy, and K. Wang
Geological Survey of Canada
Pacific Geoscience Centre
9860 West Saanich Road,
Sidney, B.C. V8L 4B2

Phone: 250-363-6447
Fax: 250-363-6565
dragert@pgc.nrcan.gc.ca

Final Technical Report
USGS 06HQGR0151

DYNAMICS OF EPISODIC TREMOR AND SLIP ALONG THE CASCADIA MARGIN

H. Dragert, H. Kao, G.C. Rogers, J. Cassidy, and K. Wang
Geological Survey of Canada
Pacific Geoscience Centre
9860 West Saanich Road,
Sidney, B.C. V8L 4B2

Phone: 250-363-6447
Fax: 250-363-6565
dragert@pgc.nrcan.gc.ca

Abstract:

Based on seismic and GPS observations along the Cascadia Margin, Episodic Tremor and Slip (ETS) is currently defined empirically as repeated, transient ground motions at a plate margin, roughly opposite to longer-term deformation motion, accompanied by distinct low-frequency, emergent seismic signals. Although the specific physical processes that give rise to ETS are still not well understood, detailed observations from this study establish new aspects of the nature of this phenomena. The striking similarity and regularity of prolonged (longer than 5 days) episodes of ETS in northwestern Washington State and southern Vancouver Island (VI) continues to be observed. Based on observations of 11 ETS episodes at the Victoria continuous GPS station, the average surface displacement is 4.9 ±0.7mm at an azimuth of -113 ±8 degrees, with a return period of 14.8 ±1.3 months. This return period has been substantiated back to 1982 from an examination of tremor episodes recorded on regional analogue seismograms. These prolonged ETS episodes in this region invariably encompass activity that migrates along the strike of the coastal margin at a velocity of 5 to 10km per day. These characteristics suggest a deeper interplate fault asperity that is spatially stable but weak and subject to repeated slow slip that propagates along strike of the subducting plate interface.

Detailed examination of seismic and deformation data for central and northern VI reveals a less regular behaviour for ETS. Tremor occurrences continue to be positively correlated with the presence of subducted slabs with the majority of tremors occurring between 25 to 45 km depth and in places where seismicity is sparse or absent. Besides the "steady" along-strike migration and "halting" behaviour found in previous prolonged ETS events in southern Vancouver Island, a pattern of "jumping" behaviour for tremor activity is clearly seen in the northern and central regions. Visual inspection of previous seismic records suggests that the jumping behaviour is probably common to ETS tremors in all regions of VI although crustal displacements have yet to be resolved with GPS for these more random, short-duration, jumping tremors. The question of whether these more isolated tremors are associated with plate slip that is more limited in magnitude or spatial extent has been addressed by examining data from borehole strainmeters (BSM) recently installed as part of Earthscope's Plate Boundary Observatory. BSM data are consistent with crustal strain generated by limited slip events supporting the hypothesis that asperity size and strength dictates the temporal behaviour of slow slip on the deeper Cascadia subduction interface.

1. Introduction

Over the past 15 years, analyses of data from continuous GPS stations in coastal southwestern British Columbia and northwestern United States show that long-term elastic deformation occurs along the northern Cascadia Subduction Zone (CSZ) due to the locking of converging plates across a portion of the subduction interface between the Juan de Fuca plate and the overlying North America (NA) plate [cf. Mazzotti et al., 2003]. The pattern of the regional crustal velocity field along the Cascadia Margin has been used to establish both block motions and the location, extent, and strength of coupling of the locked fault zone of the CSZ [cf. McCaffrey et al., 2007]. However, over the past 7 years, it has become clear that portions of the Cascadia forearc experience repeated periods of transient motion opposite to the long-term deformation and these brief reversals of motion, which can be modeled by slow slip on the deeper plate interface, are accompanied by distinct seismic tremors [Rogers and Dragert, 2003]. It has also been established that this phenomena, called Episodic Tremor and Slip (ETS), is not uniform along the length of the Cascadia margin [Szeliga et al., 2004; Brudzinski and Allen, 2007]. Consequently, a principal objective of this study was to better resolve systematic differences of ETS along the northern CSZ and thereby investigate the possible influence of crustal structure, regional seismicity, and along-strike variations in subduction geometry and plate convergence rate on ETS activity. This improved resolution of the character of ETS was enabled by improved precision of tremor locations using the "source scanning algorithm" (SSA) [Kao and Shan, 2004], the examination of analogue seismic records predating GPS coverage, and the analysis of strain data from borehole strainmeters (BSM's) recently installed as part of the Plate Boundary Observatory under the Earthscope program.

2. Data Sources

Figure 1: Location of instrumentation for monitoring deformation associated with ETS events along the northern Cascadia Margin. White circles with labels show existing regional continuous GPS stations from the WCDA, PBO, and PANGA networks. Yellow circles show locations of additional GPS sites installed under this project for the explicit study of ETS. Blue squares show PBO borehole strainmeters installed in 2005.

Figure 1 shows the sites used for monitoring crustal motions or strain associated with ETS events in the northern CSZ. New continuous GPS stations were installed under this project to help constrain the location and magnitude of slip associated with the ETS activity under Vancouver Island. Also, for the first time, extremely sensitive strain measurements from borehole strainmeters installed as part of the Plate Boundary Observatory were available to help investigate the processes involved in ETS. Figure 2 shows the coverage of seismic instruments in this region of the CSZ.

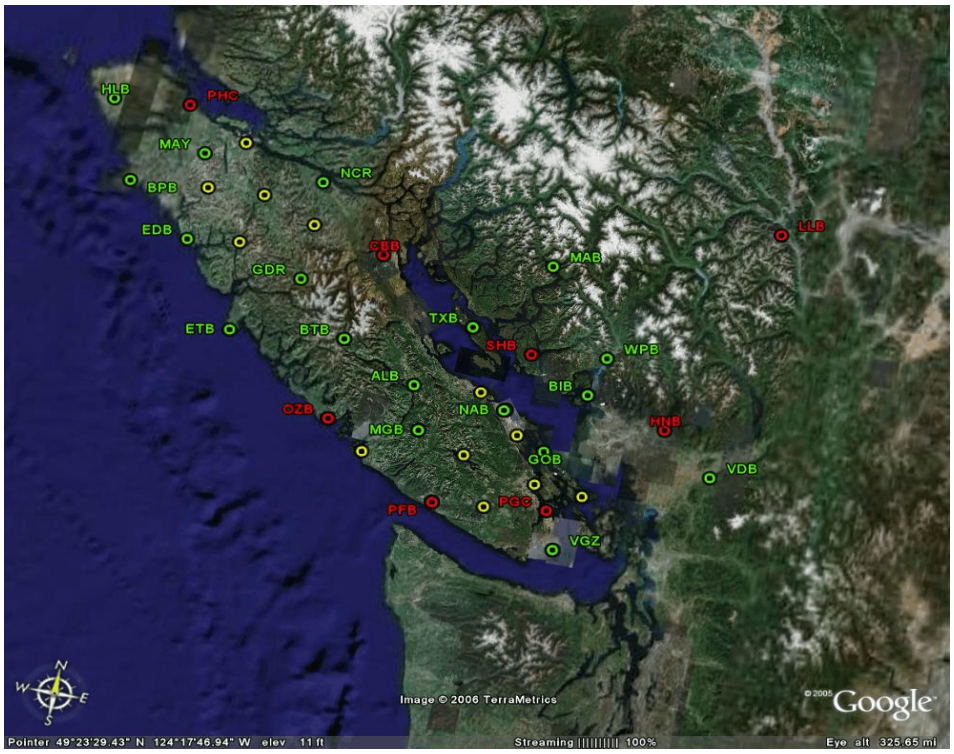

Figure 2. Seismometer coverage for monitoring ETS events along the northern Cascadia Margin. Red and green circles with labels show existing regional seismic network stations, broadband and single-component respectively. Yellow circles show locations of new seismic sites on Vancouver Is. added explicitly for the study of ETS.

This densification of seismic instruments has enabled improved location of tremor events, especially in northern and central Vancouver Island. Furthermore, analogue seismograms from long-running stations of the Canadian National Seismic Network located on southern Vancouver Island (VGZ, PGC, PFB, NAB) were examine in order to document the occurrence of tremor episodes back to 1982, thereby doubling the time-period used to determine the recurrence interval of pronounced ETS episodes in this region.

3. Character of ETS in NW Washington State and Southern Vancouver Is.

Since the discovery of "silent" slip on the CSZ by Dragert et al. [2001], the analysis of continuous GPS data from the Victoria GPS site (ALBH) from 1994 to 2007 shows that this station's motion relative to the North America plate is characterized by a sloped saw-tooth function: For periods of 13 to 16 months, there is eastward motion that is more rapid than the long-term rate, followed by a 1 to 3 week period of reversed motion (see Figure 3). The continued regularity of these brief reversals, first pointed out by Miller et al. [2002], and the consistency of the transient displacements for each episode is summarized in Table 1 which lists the dates for the mid-points of the transients as observed at ALBH. This table, now based on 14 years of continuous GPS data, is not significantly different from that published by Dragert et al. [2004]. The recurrence interval based

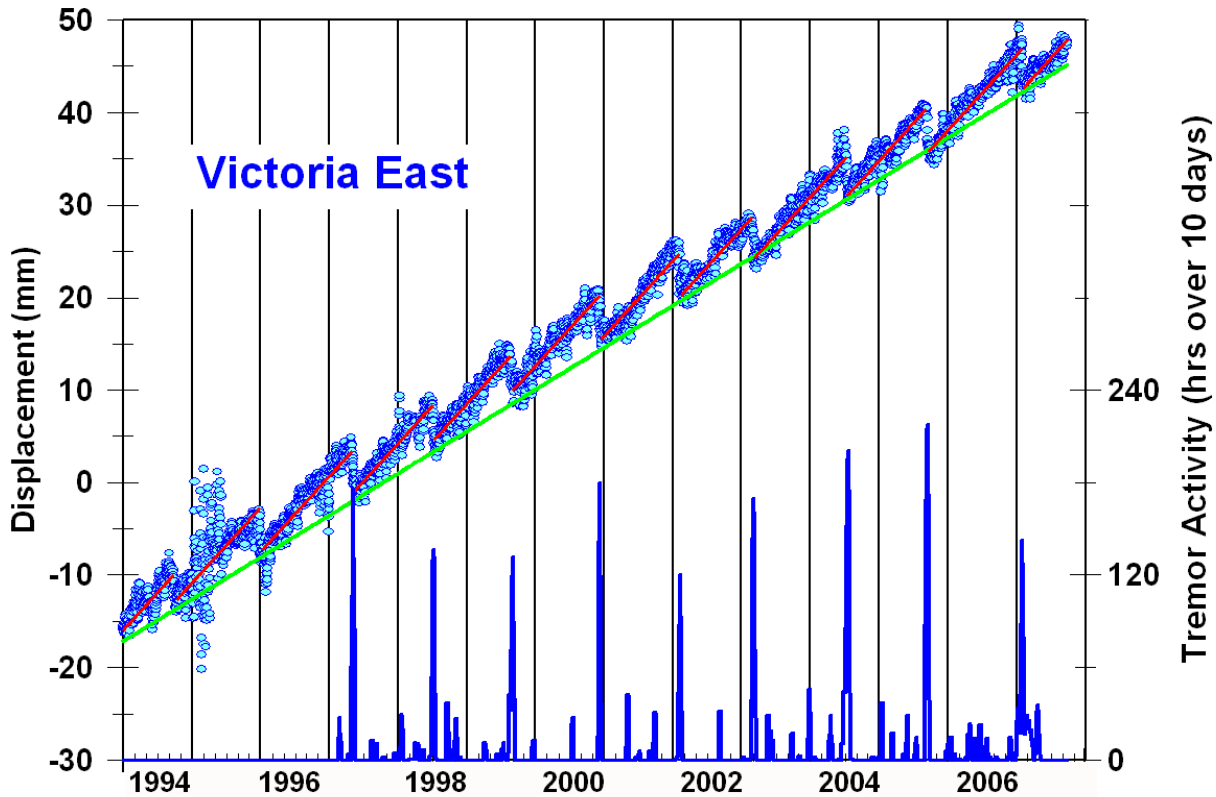

Figure 3. Sample record of slip and tremor activity observed for southern Vancouver Island. Blue circles show day-by-day change in the east component of the GPS site ALBH (Victoria) with respect to DRAO (Penticton) which is assumed fixed on the North America plate. Continuous green line shows the long-term (interseismic) eastward motion of ALBH. Red line segments show the mean elevated eastward trends between the slip events which are marked by the reversals of motion every 13 to 16 months. Blue graph at bottom shows the total number of hours containing tremor activity observed for southern Vancouver Is. within a sliding 10-day period. Tremors are also found to occur at times between slips, but tremor activity at such times is substantially less.

Table 1: GPS Transients Observed at Victoria, B.C.

Secular Velocity: 5.58 mm/yr ± 0.02 51.6 ^{o} ± 0.2

Inter-Slip Velocity: 9.44 mm/yr ± 0.10 57.9 ^{o} ± 0.6

Date	Days Between Transient	Horizontal Displacements Amount (mm)	Sigma (mm)	Azimuth (Degr.)	Sigma (Degr.)
10/02/94		3.45	0.29	-118.1	4.6
12/29/95	453	6.00	0.21	-126.4	1.9
05/08/97	496	4.95	0.19	-108.6	2.0
07/08/98	426	4.55	0.21	-119.4	2.4
08/26/99	414	4.41	0.20	-112.1	2.3
12/08/00	470	5.56	0.26	-117.2	2.5
02/06/02	425	5.09	0.19	-110.4	2.0
03/03/03	390	4.84	0.20	-103.1	2.1
07/13/04	498	4.38	0.20	- 98.3	2.0
09/11/05	425	5.31	0.20	- 113.5	2.0
01/30/07	506	4.90	0.20	- 116.0	2.2
Means:	450	4.86	0.21	-113.0	2.4
Sigmas:	38	0.65	0.03	7.5	0.7

on these GPS data is 450 ±38 days with an average surface displacement of 4.9 ±0.7 mm in an azimuthal direction of -113 ±8 degrees which is opposite to the long-term (decadal) deformation direction of the coastal margin.

The recurrence interval has now been further confirmed by identifying the onset of tremor episodes on analogue seismograms dating back to 1982. The results are shown in Table 2. The 1990 event is a significant outlier by occurring so soon after the previous event, thereby creating two anomalous, brief intervals. From its character on the helicorder records, this event seems typical in every way, but by omitting it, the statistical properties are more likely representative of the occurrence behaviour over the last 25 years. Thus 430.9 days (or 14.3 months) with a 95% confidence interval (2 sigma) of 88 days is the preferred interpretation.

For comparison, the average recurrence interval for the last 11 events, which were also recorded by GPS, has also been calculated. The results are identical to the GPS determinations. This shows that using the onset times of the tremors or the mid-point times of the surface displacements yields the same values implying that the duration of each episode has a minimal effect on the estimate of the average interval.

The location of tremor sources and the character of tremor migration observed for the 2003 and 2004 ETS episodes in this region [Kao et al., 2006] are again replicated in the September 2005 ETS episode. Figure 4 shows the horizontal and depth distribution of tremor sources from Sep. 4 to Sep. 26 as determined by the "Source Scanning Algorithm" (SSA) [Kao and Shen, 2004]. The horizontal locations have been mapped into a coordinate system with the y-axis at 51.4 degrees west of north and the x-axis 38.6 degrees north of east, with the origin approximately at N49.38, W125.16 (about 24 km northwest of Port Alberni on Vancouver Island). In this axis orientation, it is clear that the horizontal distribution for tremor source locations is over a northwest trending strip about 40 to 50 km wide with a migration velocity of about 8 km per day in a northwest direction. As in previous tremor episodes analyzed for this area, the depth distribution is from 5 to 45 km with no apparent depth migration on a day-to-day basis. Note that the 386 tremor locations plotted represent not all but only the strongest and best-located events.

Table 2: ETS tremor events on southern Vancouver Is. from seismograms

Start Date	*Julian Day*	*Interval(days)*	
1982 Jun 20	(171)		
1983 Aug 18	(230)	424	
1984 Nov 15	(320)	455	
1986 Jan 02	(002)	413	
1987 Feb 17	(048)	411	
1988 Mar 17	(077)	394	
1989 Apr 21	(111)	400	
?**1990** Nov 25	(330)	219	
1991 Aug 14	(226)	261	
1992 Jul 08	(190)	329	
1993 Aug 12	(224)	400	
*1994 Sep 23	(266)	407	
*1995 Dec 24	(358)	457	
*1997 Apr 29	(119)	491	
*1998 Jun 28	(179)	425	
*1999 Aug 14	(226)	412	
*2000 Dec 2	(337)	475	
*2002 Feb 2	(033)	427	
*2003 Feb 25	(056)	388	
*2004 Jul 08	(190)	499	
*2005 Sep 03	(246)	422	
*2007 Jan 24	(024)	508	
	All	***-1990***	****GPS***
Mean (days)	410.3	430.9	450.5
Sigma (days)	70.6	44.2	38.6
No. of events	22	21	11

bold are identified from helicorder records
? is anomalous event
** has GPS confirmation*

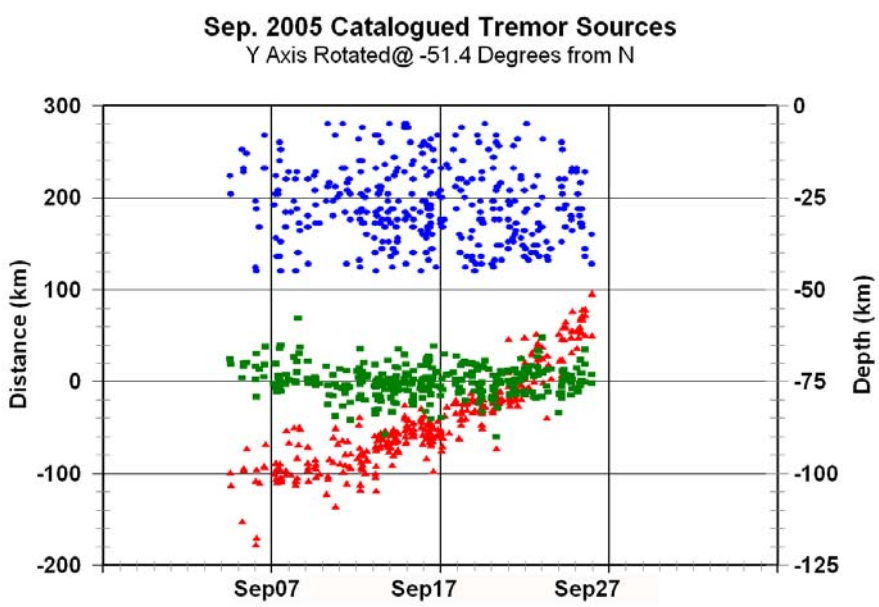

Figure 4. Tremor source locations for the September 2005 ETS episode. Coordinates of the locations have been determined with the SSA technique and plotted in a rotated coordinate system where red triangles are roughly the NW, green squares the NE, and blue circles the depth components.

4. Character of ETS in Northern and Central Vancouver Island

In contrast to the tremendous progress toward the characterization and understanding of ETS events in the region of southern VI and Washington State [Kao, et al., 2005; Kao, et al., 2006; McCausland, et al., 2005; Melbourne, et al., 2005; Rocca, et al., 2005], there has been little detail on the spatial and temporal distribution of ETS tremors in the northernmost Cascadia margin where the Explorer plate (EP) and northern Juan de Fuca (JDF) subduct beneath North America (NA). In these regions, the subducting plate is younger and warmer and the relative convergence between EP and NA is very slow (<~2 cm/yr) [Braunmiller and Nábelek, 2002]. Farther to the southeast, JDF is moving at ~4 cm/yr with respect to NA, causing left-lateral movements along the Nookta fault zone (NFZ) that defines the transform boundary between JDF and EP. Based on seismic receiver function analysis, Cassidy et al. [1998] found no subducted slab to the northwest of Brooks Peninsula, a situation that has persisted for tens of millions of years [Lewis, et al., 1997]. The distribution of local earthquakes indicates that most seismicity occurs offshore and is probably associated with the tectonic deformation along or in the vicinity of plate boundaries [Braunmiller and Nábelek, 2002; Cassidy and Rogers, 1995; Hyndman and Rogers, 1981]. Both the overriding crust and the subducted slab beneath the northern and middle VI are basically aseismic.

As part of this study, we determine the origin times and hypocenters of two seismic tremor sequences that occurred in April and May 2005 in the region of northern and middle VI. Specifically, we address three issues: 1) is there a northernmost (geographic) limit in the distribution of Cascadia ETS tremors? 2) is there any significant variation in the spatial and temporal patterns of ETS tremors for different parts of VI? and 3) does the change of subduction parameters (e.g., the age of subducted slab and relative convergence rate) affect the distribution of tremors? We discuss the possible implications of our observations to the seismogenic mechanisms of ETS tremors in our conclusions.

4.1 Horizontal Distribution

Figure 5 shows the overall spatial and temporal distribution of tremors for this time period. There were two distinct episodes in the two month period (April and May 2005) with a time gap of 3 weeks in between. The first one (referred as the April episode, red dots in Figure 5a) lasted 12 days from April 19 to 30, 2005, whereas the second one (referred to as the May episode, blue dots in Figure 5a) was observed during May 21–30, 2005. The most striking feature of our observations is the sudden "jumps" of tremor clusters from one region to another within the same episode, a pattern in sharp contrast to the gradual along-strike migration documented for southern VI. While this "jumping" behaviour has been suspected from sudden changes in the maximum amplitudes of observed waveforms, this is the first time it is documented with precise locations. For examples, ETS tremors in the first two days of the April episode (April 19 and 20) were mainly clustered in the northern VI region (Figure 5b). In the next two days (April 21 and 22), the level of tremor activity in the north dropped to a complete quiescence, while another group of tremors occurred ~100 km to the southeast. The occurrence of tremors jumped back to the north afterwards, and the distribution remained almost stationary until the end of April (Figure 5b). The tremor activities in the two regions (i.e., before and after a jump) occurred in a mutually exclusive fashion. To further verify that such mutual exclusiveness is not an artifact due to the inability and/or insufficient resolution of our SSA analysis, we carefully re-examined and compared all seismic waveforms recorded by stations located in northern and middle VI on April 20 and 21. The clear contrast in the waveform characteristics unambiguously confirms our observation.

A similar jumping behaviour was also observed in the May episode (Figure 5c). During the first 6 days (May 21–26), all tremors were located in middle VI. Then, the tremor activity shut off completely for one day. When the tremor activity resumed on May 28, 2005, the majority of them were located ~200 km to the southeast near the southern tip of VI (Figure 2c). Unlike the April

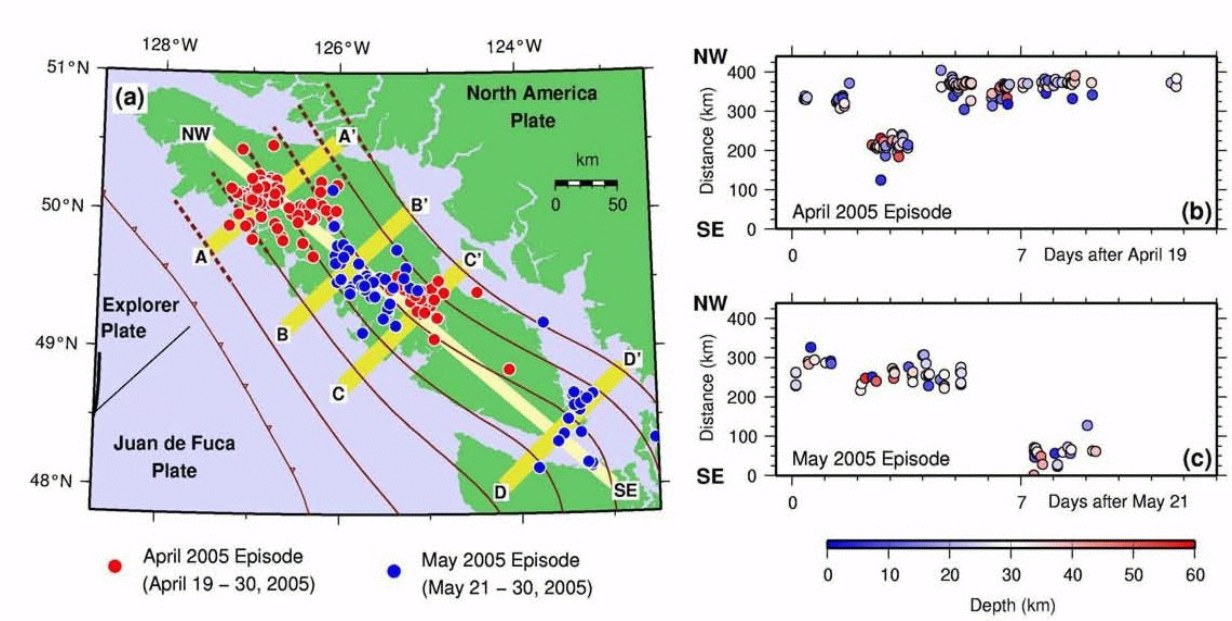

Figure 5. Spatial and temporal distributions of the two tremor episodes observed in northern and middle Vancouver Island. (a) Each dot represents one tremor solution. Red and blue colours correspond to the April and May 2005 episodes, respectively. Notice that the vast majority of tremors in the May episode are located in places unoccupied by the April episode. (b) Time-location plot for the April 2005 tremor episode. Each tremor location is projected onto a NW–SE profile roughly parallel to the strike of the plate interface. The horizontal axis corresponds to time relative to the beginning of the episode. Different colours represent different source depths, as shown by the Collor scale. The episode started in the north, but suddenly jumped ~100 km to the southeast for two days, then jumped back. (c) Time-location plot for the May 2005 tremor episode. This episode began by filling the gap left by the April episode in middle Vancouver Island. Toward the end of this episode, the activity suddenly jumped to the south by ~200 km.

episode, the May tremor episode stayed there until the end of this sequence (May 28–30) and never returned to middle VI. Interestingly, we notice that the area corresponding to the main group of the May episode (i.e., tremors occurred during May 21–26) matches remarkably well with the spatial gap left by the April episode (Figure 2a). At this moment, it is probably premature to conclude that the "gap-filling" behaviour by the next tremor sequence in the adjacent segment is a repeating process more common to all other Cascadia tremor episodes or just a one-time coincidence. Nevertheless, this observation strongly suggests a possible interaction between two ETS events that occurred closely in both time and space. Finally, no tremors occurred in the northernmost part of VI which is outside of the northern limit of the subducted Explorer slab. The fact that all ETS tremors are located within the span of the subduction zone is compatible with the interpretation that fluids released from dehydration of subducted materials are directly or indirectly involved in tremor generation, as proposed by many previous studies [e.g., Dragert, et al., 2004; Kao, et al., 2005; Kao, et al., 2006; Obara, 2002; Seno and Yamasaki, 2003].

4.2 Depth Distribution

We constructed four cross sections from north to south to show the vertical distribution of seismic tremors at various times and locations (Figure 6). All cross sections are oriented perpendicular to the strike of the subducted plate (see Figure 5). Only events within 15 km from each profile are plotted to prevent distortion from lateral projection over a long distance. Profiles A–A' and B–B' correspond to the main groups of the April and May episodes, respectively, whereas profiles C–C' and D–D' are devoted to the "jumped" groups. In addition to seismic tremors,

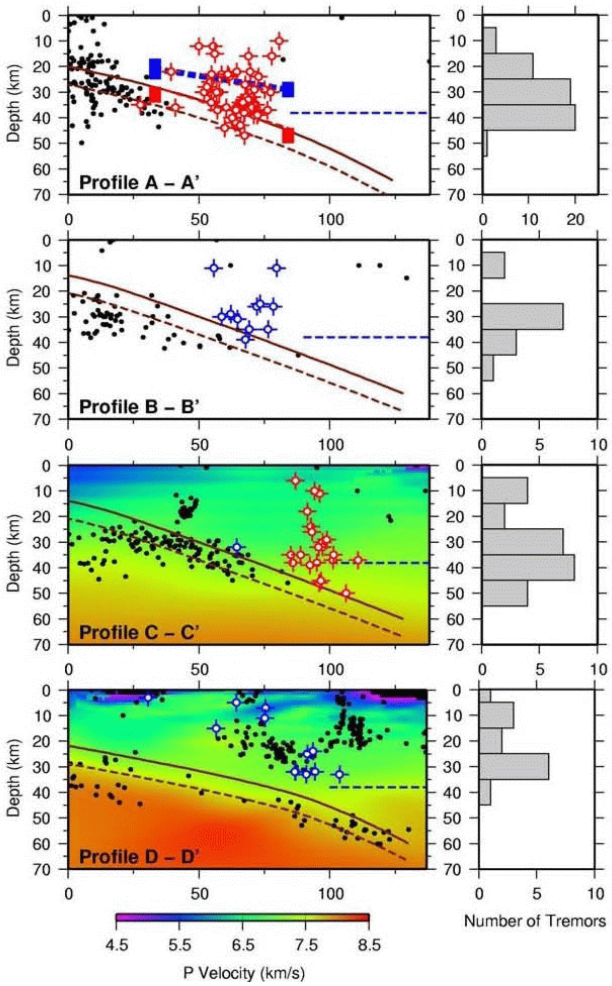

Figure 6. Cross sections showing the depth distribution of seismic tremors (open dots with crosses) in the April (red lines) and May (blue lines) 2005 episodes with respect to the background seismicity (solid dots). Locations of profiles are shown in Figure 5a. P wave velocity distribution is shown in color for regions where local tomography is available. To avoid any distortion from projecting over a large distance, only tremors and local earthquakes within 15 km from each profile are plotted. For the northernmost profile, the low Vs zones identified from receiver function analysis are shown in red and blue boxes. The approximate locations of the plate interface, the bottom of the subducted oceanic crust, and the bottom of the continental crust are marked by solid brown, dashed brown, and dashed blue lines, respectively. Histograms to the right show the total numbers of tremors at various depth ranges along different profiles. The majority occurred between 25 and 45 km in the vicinity of plate interface or immediately above the continental Moho discontinuity. Most tremors occurred in places where local seismicity is sparse.

hypocenters of local earthquakes and available constraints on velocity models are also plotted for reference. The most noticeable pattern in Figure 6 is that tremors tend to occur in places where local seismicity is sparse or absent. For example, most local earthquakes in the north occurred offshore west of VI (profile A–A'). The majority of seismic tremors in the April episode, however, are located inland where both the subducted slab and overriding crust are aseismic. Similarly, tremors in the middle VI region are located away from most local earthquake clusters, as shown in profiles B–B' and C–C' of Figure 6. Although the overriding crust in southern VI is more seismically active, the tendency of mutual exclusiveness between tremors and earthquakes seems to remain unchanged (profile D–D').

This is consistent with previous observations [Kao, et al., 2005; Kao, et al., 2006], implying fundamental differences in the seismogenesis between ETS tremors and earthquakes. Another noticeable feature is the relatively wide depth distribution of tremors in all profiles. This is again consistent with the patterns previously found for the 2003 and 2004 ETS tremor episodes in southern VI. Notice that the number of tremors at different depth ranges is by no means uniform. The majority occurred at depths between 25 and 45 km (Figure 6). In particular, more than 70% of tremors in northern VI were located immediately above the plate interface. The number of tremors above the shallower low-velocity zone (~5–15 km above the plate interface, and is interpreted as the corresponding "E" reflector found in the south) is significantly less. This uneven depth distribution seems to be true for both the main and "jumped" groups.

4.3 Corresponding Strain Observations

Although the spatial and temporal patterns of tremor for the northern and central Vancouver Is. regions are clear, the corresponding crustal displacements have not been well resolved by the GPS coverage currently in place. For example, for the 2005 tremor sequences discussed in detail above, there were no surface displacements observed at nearby GPS sites that exceeded the day-to-day 2-sigma error level. This implies that maximum displacements accompanying these tremor sequences, if any, were less than 2 to 3 mm. This leads to a fundamental question: Are shorter and more random tremor sequences, such as those discussed above, still attributable to slip on the deeper subduction plate interface, as has been modelled for the regular, prolonged ETS episodes of souther Vancouver Is. and northwestern Washington [Dragert et al., 2004], or can tremor occur independent of slip? This question has been addressed as part of this study by examining data from borehole strainmeter recently installed on Vancouver Is. as part of the Plate Boundary Observatory (PBO) under the Earthscope program.

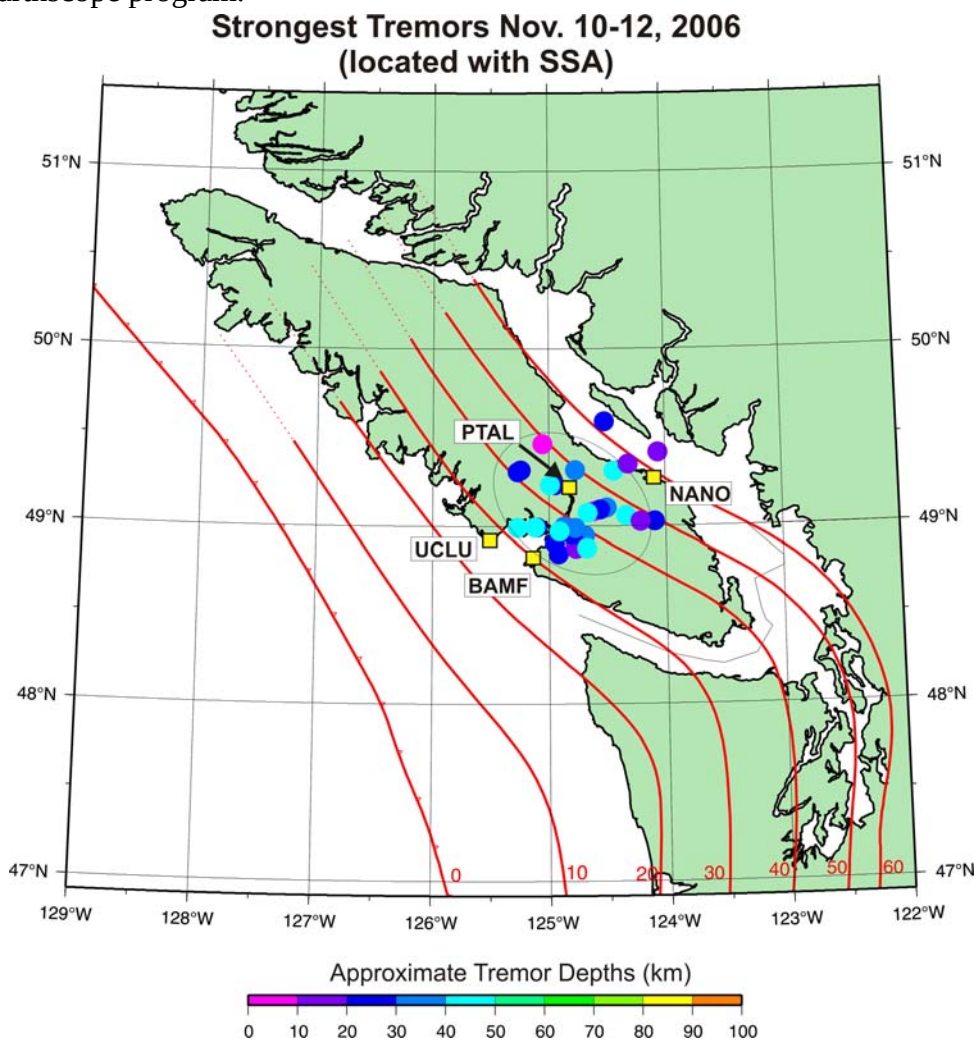

Figure 7. Tremor locations for November 2006 in the southern flank of central Vancouver Island. Tremor locations are shown by circles with colours indicating approximate depths. The ellipse shows the 90% boundary for the located tremors. Labelled yellow squares are continuous GPS stations closest to this tremor activity.

Over the period of Nov. 9 to 13, a significant burst of tremor activity occurred in the central Vancouver Island region (Figure 7). However, the closest GPS sites to this region of tremors showed very small or no horizontal displacements during this period (Figure 8). Estimates of daily vertical

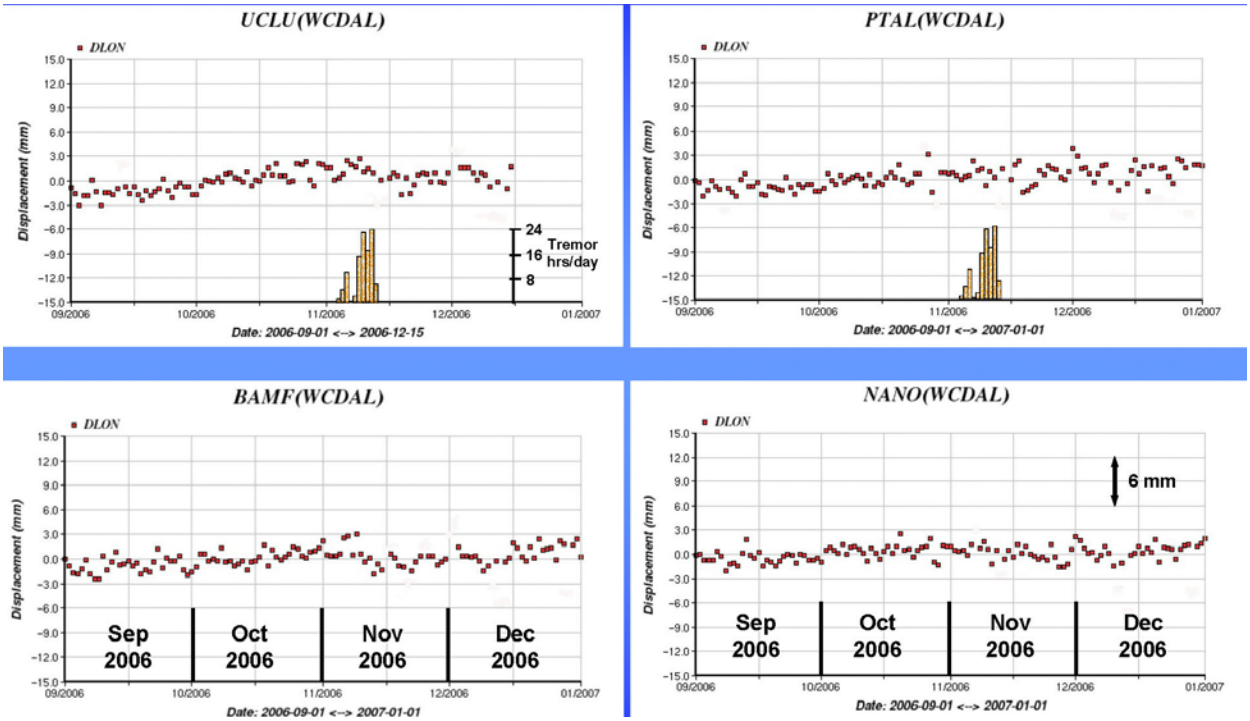

Figure 8. Daily variations of the east components at continuous GPS stations in the Nov. 2006 tremor region. Positions are estimated with respect to Penticton (DRAO) which is assumed fixed on the North America Plate. The orange bar graph replicated in the upper two panels show the total number of hours during a day that contain tremor activity. UCLU and BAMF show possible displacements coincident with the tremor occurrences, but amounts are less than 3 mm which lies within the 2-sigma error level.

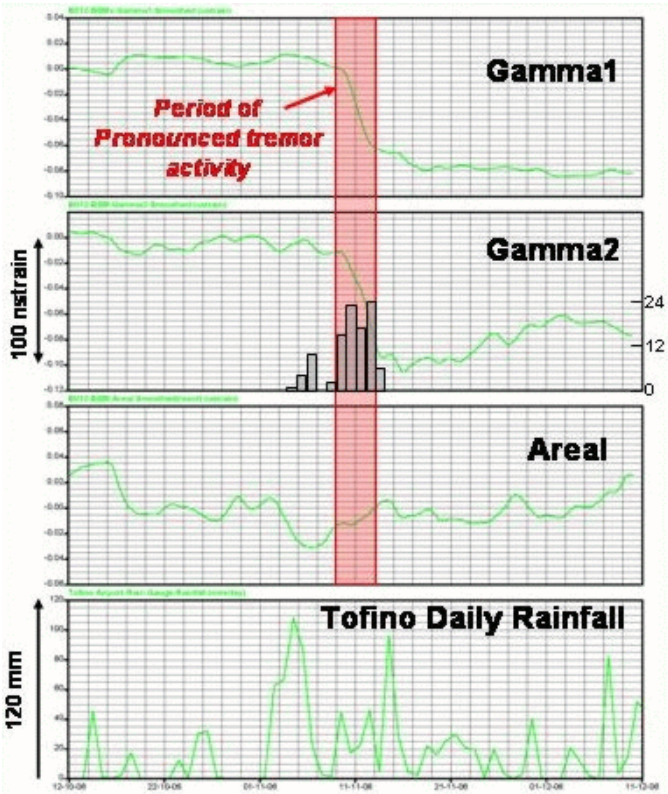

Figure 9. Transient strain changes observed at B012 located at UCLU. The top 3 panels show the observed strain with 2-day smoothing applied. The bottom panel shows daily regional rainfall. Tremor activity from Figure 8 is replicated in panel 2.

positions for these sites were unusually noisy during this period because of record breaking amounts of rain enhancing multipath effects and degrading tropospheric delay estimates.

Fortunately, a PBO borehole strain-meter (BSM) had been installed at the Ucluelet GPS site (UCLU) in the fall of 2005, and it recorded a transient signal in the shear-strain components coincident with the tremor activity. Figure 9 shows the observed strain components with 2-day smoothing applied. The areal strain (panel 3) has also been corrected for atmospheric pressure variations. The approximate magnitudes of the changes in strain over the 4-day period of more intense tremor activity were -65, -80, and +20 nano-strain in the gamma1, gamma2, and areal strain respectively. The total rainfall in the region, which peaked to over 100mm on some days is shown at the bottom of Figure 9. The residual areal strain correlates with the implied increase in ground hydrostatic loading (increased rain results in areal compression, which is negative by convention). It is therefore possible that the

20 nanostrain of extension attributed to the strain signal likely associated with ETS could be larger but is masked by the rainfall loading.

To model the observed strain we use the subducting plate geometry adapted from Flueck et al. [1998] and Wang et al. [2003], where the bottom of the transition zone on the subducting plate interface has been augmented by a "slip zone" where episodic slow slip is thought to occur. We consider slip in an elastic half-space on a small slip asperity at an average depth of about 35 km on the plate interface, since models of slip for pronounced ETS events under southern Vancouver Island and the Olympic Peninsula have shown surface GPS displacements consistent with slip at these depths. Clearly the geometry of the slip area and the distributions of slip are not uniquely constrained by the available deformation data. We found a simple circular (~30 km in diameter) asperity with a uniform updip slip of 3 cm will replicate the observed strain transient and result in less than 3 mm surface displacement at the coastal GPS stations, UCLU and BAMF. However, such a small asperity, although it cannot be ruled out, is definitely at odds with the wider distribution of the observed tremors shown in Figure 7.

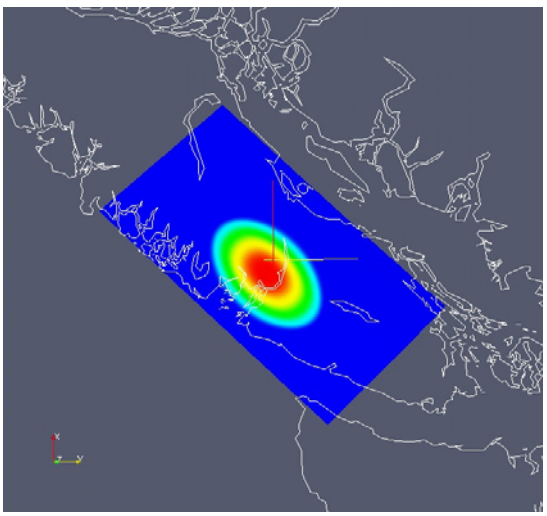

Figure 10. Elliptic slip asperity on the subducting plate interface. The ellipse has a major axis of 90 km, a minor axis of 60 km, an average depth of 38 km, and a bell-shaped distribution of slip that has a maximum magnitude of 3 cm.

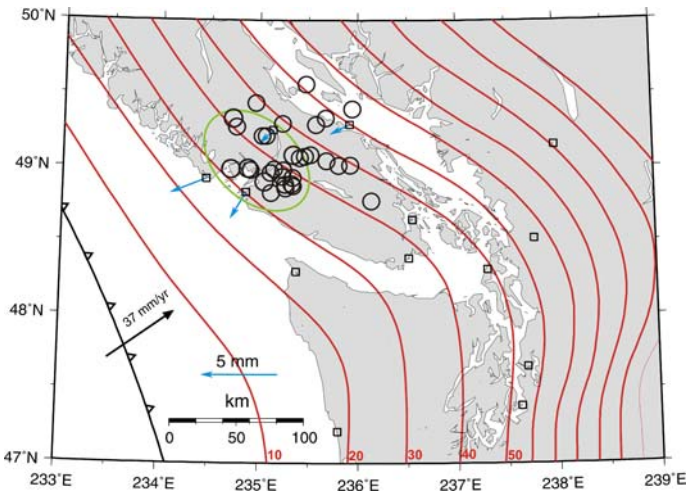

Figure 11. Predicted surface displacements at existing regional GPS sites. Green ellipse shows the location of the slip region described in Figure 10. Red lines are depth contours to the top of the subducting plate. Black circles are the tremor locations from Figure 7.

Consequently, we also modeled a larger elliptical slip region with a major axis of 90 km aligned in a northwest direction, a minor axis of 60 km, a mean depth of 38 km, and a bell-shaped slip distribution with maximum slip of 3 cm (see Figure 10). The surface displacements for this model at the regional GPS sites are shown in Figure 11 and the surface horizontal strain components are shown in Figure 12. The model predictions are consistent with the observed data indicating that the true slip asperity is not well constrained and multiple fault shapes and sizes can replicate the observations. Nonetheless, it is clear that smaller and more randomly occurring episodes of tremor are accompanied by crustal strain changes that are not well resolved by GPS but are observable by PBO BSM's. Furthermore, it is significant that even with the larger elliptical slip area, the horizontal distribution of the tremor sources is greater (see Figure 11). The implication is that tremor associated with slip on the deeper plate interface can be located well away from the region of maximum slip.

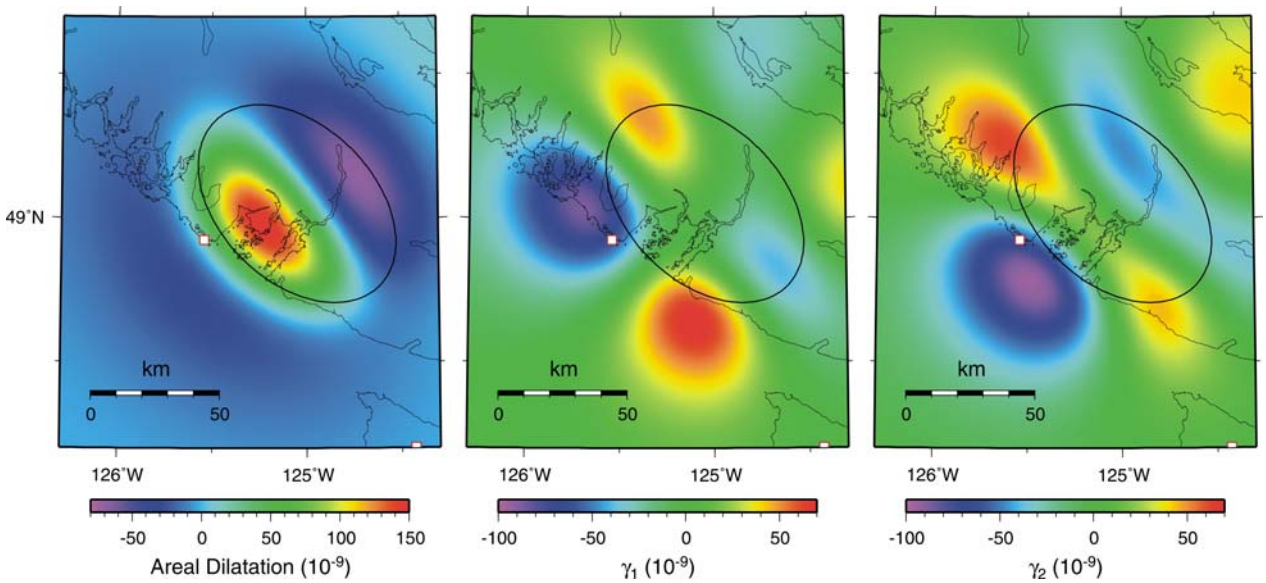

Figure 12. Surface strain components for slip on the elliptical patch described in Figure 10

5. Discussion and Conclusions

For the region of southern Vancouver Is. and northwestern Washington State, the regular recurrence interval of 14.7 months has been corroborated from analogue seismographs dating back to 1982. Also, the uniformity of crustal displacements at Victoria continues to be observed in the most recent (Sep. 2005, Jan. 2007) ETS events. It is difficult to envisage such regularity arising from a process where shear is distributed throughout the crust. Rather this regularity suggests the existence of a uniform, spatially stable, low-strength asperity on the subducting plate interface spanning depths from 25 to 45 km. Temperatures of 450 to 550°C and an abundance of fluids from dehydrating metabasalts [Peacock, 1990] determine the mechanical, rheological, and dynamic properties of the subduction fault at these depths. Although more random bursts of ETS have been observed for this region as well, its dominant mode for slow slip is in prolonged regular episodes where slip and tremor activity migrate, continuously or haltingly, along the strike of the subduction zone [Kao et al., 2006]. This further suggests a relatively smooth asperity that is conducive to the propagation of slow slip where the propagation speed is governed by pore pressure [Liu and Rice, 2005] not structural features.

The detailed study of the April and May 2005 tremor activity in northern and central Vancouver Is. reveals a third type of tremor migration pattern. In southern VI, two common types of migration patterns have been documented. The first one is “steady” migration, where slip and tremors migrate from southeast to northwest at a relatively steady speed [e.g., Kao, et al., 2006; Rogers and Dragert, 2003]. The second one involves “halting” behaviour during which the locations of slip and tremors stay in a particular place (sometimes with a subsided level of activity) for a short period of time before the migration resumes. The temporary halt can last from several days - e.g., the March 2003 and July 2004 ETS events [Kao, et al., 2006], or possibly to two weeks - e.g., the August1999 ETS event [Dragert et al., 2004]. In this study, we report the third type of tremor migration patterns, i.e., the “jumping” behaviour. Figure 13 schematically illustrates the three different types of ETS migration patterns (i.e., steady moving, halting, and jumping) that have been observed so far in northern Cascadia. While the two ETS episodes displaying this behaviour occurred mainly in the northern and middle segments of VI, this does not necessarily imply that the jumping behaviour is only limited to these geographic regions. In fact, based on visual inspection

of CNSN seismograms recorded during many previous ETS episodes, it seems that sudden jumps in the location of tremor clusters might have happened at least three times before in middle and southern VI (the April/May 1997, December 2000, and January/February 2002 episodes). We speculate that the jumping behaviour is common to ETS tremors in all regions of VI and northwestern Washington, likely caused by slip over small asperities that were excluded in a previous slip episode.

Evidence that the shorter periods of tremor, such as the "jumping" episodes described above, can still be associated with deep slow slip has been provided by borehole strainmeter data. Strain patterns observed can be replicated by elastic slip dislocation on simple asperities located on the deeper plate interface, suggesting that shorter (more random) and prolonged (more regular) ETS events are identical in nature, differing mainly in the size of the slip asperity. Hence, the suggestion is that for the Cascadia Subduction Zone, ETS is a ubiquitous, on-going process, and not all regions need be characterized by regular return periods. In addition, the shear strain observed at the single BSM in this study presents an inconsistency if a tighter spatial correlation is to be maintained between the tremor and slip regions. Spatial extents for tremor that are significantly greater than slip asperities, as well as the extensive depth distribution of tremors, suggest dissimilar source regions.

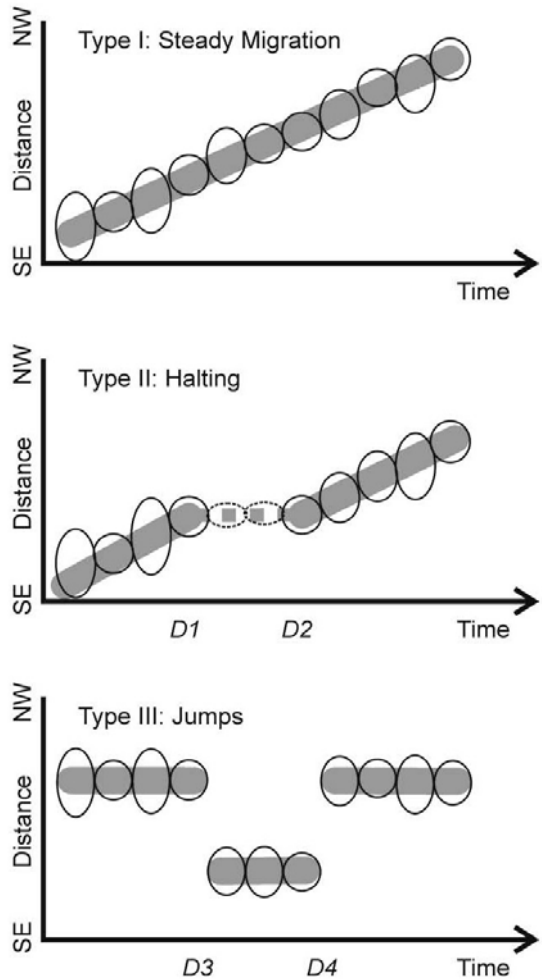

Figure 13. Schematic diagram showing the three types of tremor migration in northern Cascadia. Each oval represents the approximate daily distribution of tremors. The thick gray lines show the tremor migration paths with respect to time (horizontal axis) and coast-parallel distance (vertical axis). Type I (top panel) shows steady migration Type II (middle panel) shows "halting" behaviour, where there is a pause in the propagation during which a subsided level of tremor activity may also be observed (indicated by the dashed ovals). Type III (bottom panel) shows "jumps" of tremor clusters. In this case, the daily tremor distribution can suddenly shift by more than 100 km to the adjacent segment (D3). The tremor cluster may jump back to its original location after a while (D4), or it can stay there until the end of this episode.

The uneven depth distribution is a common feature for all regions (Figure 6). The number of tremors reaches a peak at the depths between 25 and 45 km, roughly corresponding to a 15-km-thick zone above the plate interface, with fewer occurrences in the overriding crust above and subducted crust below. We dismiss the suggestion that the wide depth range is a result of uncertainty in our analysis because the observed data clearly indicate the existence of tremors at both shallow and deep depths [see Kao et al., 2006]. If the occurrence of tremors is strongly influenced by the presence of fluids in the source region, then perhaps the spatial patterns of tremors are more associated with how the fluids in the subduction system are ultimately distributed in the overlying crust and not with structural features such as the subducting plate interface. From seismic reflection studies, Nedimovic et al. [2003] have identified such fluid inclusions which appear as strong shear reflectors in the southern Vancouver Is. region at depths of 15 to 30 km.

In summary, findings from this study re-enforce our preferred conceptual model presented in Kao et al. [2006]: ETS tremors are the manifestation of hydro-seismogenic processes in response to the temporal variation of stress field associated with the episodic slip along the lower portion of the plate interface downdip from the locked zone. The temporal dilatational stress field from episodic slips may enhance the migration and/or diffusion of fluids away from the interface. However, because no tremor migration upward from the interface has yet been resolved on a day-to-day basis, the migration/diffusion of fluids is probably not directly responsible for the occurrence of tremors. Instead, the tremors are probably "triggered" by the temporal stress variation in the fluid-rich region where seismogenesis is already close to the critical state and the distribution of fluid inclusions govern the nature of the shearing thought to be associated with tremors.

In conclusion, the implications of the ETS findings from this study for seismic hazard are not novel. The geographic distribution of tremors overlies the 25 to 45 km depth contours of the subducting plate, no matter which mode of migration, and it does not extend north of the northern edge of the Explorer Plate. This corroborates the link between tremor activity and subduction dynamics and supports using the updip limit of the ETS zone as a proxy for the downdip limit of rupture for the next megathrust earthquake [Dragert et al., 2004]. However, making practical use of the hypothesis that the likelihood of a megathrust earthquake is enhanced at the time of and immediately after ETS activity [Mazzotti and Adams, 2004] becomes more difficult. Although it can been demonstrated that a deep slip event moves the shallow locked zone closer to rupture, the question now must include: What size and duration of slow-slip is likely to be significant in terms of possible triggering of megathrust rupture? Finally, the observation that most tremors occurred in places where local seismicity is sparse for both northern/mid Vancouver Is. (this study) as well as southern Vancouver Is. [Kao et al., 2006] poses simple but significant seismic hazard questions: 1) What is the relationship between tremors and crustal seismicity? 2) Do tremors relieve crustal stress? and 3) Are the crustal regions that mark a transition from seismic to tremor activity more likely to give rise to large (M=7) crustal earthquakes? These questions await further research.

References

Braunmiller, J., and J. Nábelek , Seismotectonics of the Explorer region, *J. Geophys. Res.*, **107**, doi:10.1029/2001JB000220, 2002.

Brudzinski, M.R., R. M. Allen, Segmentation in Episodic Tremor and Slip all along Cascadia, *Geology*, in press, 2007.

Cassidy, J. F., and G. C. Rogers, The rupture process and aftershock distribution of the 6 April 1992 Ms 6.8 earthquake offshore British Columbia, *Bull Seismol. Soc. Am.*, **85**, 716-735, 1995.

Cassidy, J. F., R. M. Ellis, C. Karavas, and G. C. Rogers (1998), The northern limit of the subducted Juan de Fuca plate system, *J. Geophys. Res.*, **103**, 26,949-26,961, 1998.

Dragert, H., K. Wang, and T.S. James, A Silent Slip Event on the Deeper Cascadia Subduction Interface, *Science*, **292**, 1525-1528, 2001.

Dragert, H., K. Wang, and G. Rogers, Geodetic and seismic signatures of Episodic Tremor and Slip in the northern Cascadia subduction zone, *Earth Planets and Space*, **56**, 1143-1150, 2004.

Flueck, P., R.D. Hyndman, and K. Wang , Three-dimensional dislocation model for great earthquakes of the Cascadia Subduction zone, *J. Geophys. Res.*, **102**, 20539-20550, 1997.

Hyndman, R. D., and G. C. Rogers, Seismicity surveys with ocean bottom seismographs off western Canada, *J. Geophys. Res.*, **86**, 3867-3880, 1981.

Kao, H., and S. Shan, The Source-Scanning Algorithm: mapping the distribution of seismic sources in time and space, *Geophys. J. Int.*, **157**, 589–594, 2004.

Kao, H., S.-J. Shan, H. Dragert, G. Rogers, J.F. Cassidy, and K. Ramachandran, A wide depth distribution of seismic tremors along the northern Cascadia margin, *Nature*, 436, 841-844, 2005.

Kao, H., S.-J. Shan, H. Dragert, G. Rogers, J. F. Cassidy, K. Wang, T. James, and K. Ramachandran, Spatial-temporal patterns of seismic tremors in northern Cascadia, *J. Geophys. Res.*, **111**, B03309, doi:10.1029/2005JB003727, 2006.

Lewis, T. J., C. Lowe, and T. S. Hamilton, Continental signature of a ridge-trench-triple junction: Northern Vancouver Island, *J. Geophys. Res.*, **102**, 7767-7781, 1997.

Liu, Y., and J. R. Rice, Aseismic slip transients emerge spontaneously in three-dimensional rate and state modeling of subduction earthquake sequences, *J. Geophys. Res.*, **110**, B08307, doi:10.1029/2004JB003424, 2005.

Mazzotti S., and J. Adams, Variability of near-term probability for the next great earthquake on the Cascadia subduction zone, *Bull. Seism. Soc. Am.*, **94**, 1954-1959, 2004.

Mazzotti S., H. Dragert, J. Henton, M. Schmidt, R. D. Hyndman, T. S. James, Y. Lu, and M. Craymer, Current tectonics of northern Cascadia from a decade of GPS measurements, *J. Geoph. Res.*, **108**, 2554, doi: 10.1029/2003JB002653, 2003.

McCaffrey, R., A. I. Qamar, R. W. King, R. Wells, G. Khazaradze, C. A. Williams, C. W. Stevens, J. J. Vollick, and P. C. Zwick, Fault locking, block rotation and crustal deformation in the Pacific Northwest, Geophys. J. International, doi:10.1111/j.1365-246X.2007.03371.x, 2007.

McCausland, W., S. Malone, and D. Johnson, Temporal and spatial occurrence of deep non-volcanic tremor: From Washington to northern California, Geophys. Res. Lett., 32, L24311, doi:10.1029/2005GL024349, 2005.

Melbourne, T. I., W. M. Szeliga, M. M. Miller, and V. M. Santillan, Extent and duration of the 2003 Cascadia slow earthquake, Geophys. Res. Lett., 32, L04301, doi:10.1029/2004GL021790, 2005.

Miller, M.M., T. Melbourne, D. J. Johnson, and W. Q. Sumner, Periodic slow earthquakes from the Cascadia Subduction Zone, *Science*, **295**, 2423, 2002.

Nedimovic, M.R., R.D. Hyndman, K. Ramachandran, and G.D. Spence, Reflection signature of seismic and aseismic slip on the northern Cascadia subduction interface, *Nature*, **424**, 416-420, 2003.

Obara, K., Nonvolcanic deep tremor associated with subduction in southwest Japan, *Science*, **296**, 1679-1681, 2002.

Peacock, S.M., Fluid processes in subduction zones, *Science*, **248**, 329-337, 1990.

Rocca, M. L., W. McCausland, D. Galluzzo, S. Malone, G. Saccorotti, and E. D. Pezzo, Array measurements of deep tremor signals in the Cascadia subduction zone, *Geophys. Res. Lett.*, **32**, L21319, doi:10.1029/2005GL023974, 2005.

Rogers, G.C., and H. Dragert, Episodic tremor and slip on the Cascadia Subduction Zone: The chatter of silent slip, *Science*, **300**, 1942-1943, 2003.

Szeliga, W., T.I. Melbourne, M.M. Miller, and V.M. Santillan, Southern Cascadia episodic slow earthquakes, *Geophy. Res. Lett.*, **31**, L16602, doi:10.1029/2004GL020824, 2004.

Seno, T., and T. Yamasaki, Low-frequency tremors, intraslab and interplate earthquakes in southwest Japan—from a viewpoint of slab dehydration, *Geophys. Res. Lett.*, **30**, 2171, doi:10.1029/2003GL018349, 2003.

Wang, K., R. Wells, S. Mazzotti, R.D. Hyndman, and T. Sagiya, A revised dislocation model of interseismic deformation on the Cascadia subduction zone, *J. Geophys. Res.*, **108**, 2009-2022, 2003.

APPENDIX 1

Given that the possibility of a megathrust earthquake in northern Cascadia increases during an ETS event [Mazzotti and Adams, 2004], identifying seismic tremors during the early stage of an ETS event can be highly desirable. Consequently, as part of this project, we developed a methodology for the automated detection of seismic waveforms associated with regional episodic tremor and slip. This is strictly a technological innovation that has no direct impact on the scientific findings of our study and the description of this algorithm has recently been published as follows: *Kao, H., P. J. Thompson, G. Rogers, H. Dragert, and G. Spence (2007), Automatic detection and characterization of seismic tremors in northern Cascadia, Geophys. Res. Lett., 34, L16313, doi:10.1029/2007GL030822.*
We therefore chose to keep discussion of this technique separate from the main body of our report and for completeness, include a copy of the actual publication here in an appendix. To provide a quick overview of this work, the abstract of the publication is repeated below.

"We develop an algorithm that automatically detects and characterizes seismic waveforms associated with episodic tremor and slip (ETS) events in northern Cascadia. For each hour-long seismogram, the process begins with the calculation of moving average and scintillation index functions. A logic chart is designed to sort the observed waveform patterns into a set of classes based on these functions. An ETS event is always manifest by many station-hours with coherent tremor (CT) patterns. Automatic analysis of seismic waveforms recorded in the past three years gives results consistent with the work done by tedious visual inspection of seismograms. Our algorithm, which is free from human oversight, is ideal for an automatic tremor monitoring system to give immediate notice of an ETS event."

Automatic detection and characterization of seismic tremors in northern Cascadia

Honn Kao,[1,2] Philip J. Thompson,[2] Garry Rogers,[1,2] Herb Dragert,[1,2] and George Spence[2]

Received 29 May 2007; revised 10 July 2007; accepted 24 July 2007; published 28 August 2007.

[1] We develop an algorithm that automatically detects and characterizes seismic waveforms associated with episodic tremor and slip (ETS) events in northern Cascadia. For each hour-long seismogram, the process begins with the calculation of moving average and scintillation index functions. A logic chart is designed to sort the observed waveform patterns into a set of classes based on these functions. An ETS event is always manifest by many station-hours with coherent tremor (*CT*) patterns. Automatic analysis of seismic waveforms recorded in the past three years gives results consistent with the work done by tedious visual inspection of seismograms. Our algorithm, which is free from human oversight, is ideal for an automatic tremor monitoring system to give immediate notice of an ETS event.
Citation: Kao, H., P. J. Thompson, G. Rogers, H. Dragert, and G. Spence (2007), Automatic detection and characterization of seismic tremors in northern Cascadia, *Geophys. Res. Lett.*, *34*, L16313, doi:10.1029/2007GL030822.

1. Introduction

[2] The non-volcanic seismic tremors and episodic tremor and slip (ETS) events have received increasing attention from the geophysical community since their discoveries in southwest Japan [*Obara*, 2002b] and Cascadia [*Rogers and Dragert*, 2003] about 5 years ago. The newly observed phenomena not only exhibit seismic characteristics very different from that of typical earthquakes but also are improving our understanding of seismogenic processes in subduction systems [e.g., *Kao et al.*, 2006; *Seno and Yamasaki*, 2003]. Recently, sevaral research projects have been initiated in various parts of the world to investigate the once-overlooked tremor signals, and the results are very fruitful. Episodic non-volcanic tremors are now documented for many subduction zones, including central and southern Cascadia [*McCausland et al.*, 2005; *Melbourne et al.*, 2005; *Szeliga et al.*, 2004], Costa Rica [*Broan et al.*, 2003; *Brown et al.*, 2005], Alaska/Aleutian [*Peterson et al.*, 2006], Chile [*Gallego et al.*, 2006], and New Zealand [*Douglas et al.*, 2005; *Wallace and Beavan*, 2006]. Non-volcanic tremors have also been found on the San Andreas fault [*Nadeau and Dolenc*, 2005].

[3] In southwest Japan, non-volcanic tremors are detected by cross correlating the envelopes of observed seismic waveforms [e.g., *Obara*, 2002b; *Obara and Hirose*, 2006]. This simple, yet powerful method is particularly effective when coherent tremor waveforms are recorded at many stations across a dense seismic array. The exceptionally high signal-to-noise (S/N) ratio of seismograms recorded by borehole seismometers of the Japanese networks further improves the detection capability when tremor signals are partially hidden by near-surface seismic noise [*Obara*, 2002a].

[4] Unfortunately, the envelope correlation method may not be suitable for regions without dense seismic arrays equipped with high-sensitivity borehole seismometers. Taking the northern Cascadia margin for example, the majority of permanent seismic stations are spaced at an interval of ~50 km with a mixture of surface broadband and short-period sensors. Seismic waveforms recorded with such a station distribution can vary significantly due to local effects such as different ray paths from the focal sphere, strong near-surface attenuation, and scattering phases associated with heterogeneous structures. As a result, it is rare to have coherent waveforms at many seismic stations for the envelope correlation method to succeed.

[5] The purpose of this paper is to document a quantitative system to detect and characterize seismic waveforms containing tremor signals without requiring a dense local network. A series of processing procedures are carefully designed to condition seismic waveforms recorded by isolated stations for pattern recognition and classification. The system is applied to seismic waveforms observed in northern Cascadia to show that the tremor-detection results are consistent with that of visual inspection and hence can be used to automatically monitor tremors.[1]

2. Diagnostic Functions: Moving Average and Scintillation Index

[6] We introduce two diagnostic functions that are sensitive to the overall waveform characteristics. The first one is moving average (*MA*), a simple calculation that smoothes the data and makes it easier to spot trends. In our case, we calculate the mean of the absolute amplitudes of all samples within a specific time window and assign the centre point that average value. Mathematically, it is defined as

$$ {}_i\mu_{|y|} = \left(\sum_{j=i-(N-1)/2}^{j=i+(N-1)/2} |y(j)| \right) / N \qquad (1) $$

where $|y(j)|$ is the absolute value of the normalized amplitude at point j and N is the total number of samples within a time window centered at point i.

[1]Geological Survey of Canada, Pacific Geoscience Centre, Sidney, British Columbia, Canada.
[2]School of Earth and Ocean Sciences, University of Victoria, Victoria, British Columbia, Canada.

Copyright 2007 by the American Geophysical Union.
0094-8276/07/2007GL030822$05.00

[1]Auxiliary materials are available in the HTML. doi:10.1029/2007GL030822.

[7] The second function is the scintillation index (*SI*), a parameter originally proposed to measure the intensity of energy bursts (scintillations) of radio waves in the ionosphere [*Yeh and Liu*, 1982]. It is defined as

$$SI_i = \sqrt{\left[\left({}_i\mu_{|y|^2} \quad {}_i\mu^2_{|y|}\right) / {}_i\mu^2_{|y|}\right]} \tag{2}$$

where ${}_i\mu_{|y|}$ and ${}_i\mu^2_{|y|}$ are the *MA* values of the absolute amplitude and the square of the absolute amplitude, respectively, for all sample points in a time window centered at point *i* (as defined in equation (1)).

[8] In practice, *SI* represents the square root of the normalized variance of the intensity of the signal. As a result, it increases when a change of waveform pattern is detected within the time window. The length of the time window should be at least comparable to the duration of the energy bursts to manifest the changing characteristics of waveforms. For example, for the *SI* function to be sensitive to tremor bursts of 10-s duration sampled at 10 Hz, *N* should be 101 or larger.

[9] Figure 1 demonstrates how the *MA* and *SI* functions respond to different waveform patterns. For a waveform containing typical background noise (i.e., random amplitudes fluctuating between highs and lows without any particular phases, Figure 1a), both functions remain almost flat throughout the trace. For a waveform containing spiky signals (such as a local earthquake, Figure 1b), both functions show large values as long as the spikes remain within the calculation window. However, the *SI* and *MA* functions are dramatically different for a waveform containing tremor bursts (Figure 1c). The *MA* function closely follows the waveform envelope with the maximum near the center, whereas the *SI* function exhibits two peaks with one near the onset and another near the terminus of the tremor bursts. Notice that the trough between the two peaks corresponds to the portion where the number of tremors is most abundant without a visible change of waveform pattern.

[10] The exact value of an *MA* function depends critically on how the waveform is normalized. By applying the same normalization scheme, traces containing only background noise would have relatively large *MA* values because the overall normalized amplitude for each sample is larger. In contrast, the *MA* function of a waveform containing spikes (e.g., a local earthquake) is generally small except around the spikes because most samples would have very small amplitudes after normalization. Tremor signals would give a result between these two end members (Figure 1).

3. Data Processing and Logic Chart of Pattern Classification

[11] Before the *MA* and *SI* functions of seismic waveform data are calculated, a multi-step data processing procedure must be applied to maximize the signal quality and to facilitate efficient data manipulation. First, all waveforms are cut into hour-long segments and grouped chronologically. Second, waveforms are conditioned to prevent artifacts from digital filtering. This step includes removing data glitches due to instrument noise, filling data gaps by interpolation, and removing the mean and linear trend of each waveform. Third, all waveforms are converted to ground velocity by deconvolving their respective instrument responses. Fourth, a band-pass Butterworth filter is applied with corner frequencies at 1.5 and 5 Hz to best manifest ETS tremor signals [*Kao et al.*, 2006]. Finally, each waveform is normalized to ±10 against the mean of the eight largest amplitudes (Figure 1). The decision of using the eight largest amplitudes is to prevent the normalization being dominated by an erroneous outlier in the waveform due to unknown/unwanted reasons (e.g. power or transmission instability). We have tried several different normalization factors, choosing from the six largest to the fourteen largest. Eight appeared to give the most satisfactory results that maximize the effectiveness of our algorithm in distinguishing different waveform patterns.

[12] The *MA* and *SI* functions are calculated for each hour-station seismogram using equations (1) and (2) with a time window of 10 s. We introduce two indicators to determine the pattern of a waveform. The first is the scintillation index ratio (*SIR*) which is the ratio of the maximum *SI* value to the mean value of the *SI* function, i.e.,

$$SIR = SI_{\max} / \mu_{SI} \tag{3}$$

$$\mu_{SI} = \left(\sum_{i\ 1}^{K} SI_i\right) / K \tag{4}$$

where *K* is the total number of samples.

[13] The second indicator is the mean of the *MA* function (μ_{MA}), defined as

$$\mu_{MA} = \left(\sum_{i\ 1}^{K} {}_i\mu_{|y|}\right) / K \tag{5}$$

which is a good discriminator for spiky/earthquake signals in a waveform.

[14] Qualitatively, a pattern of background noise is expected to have a *SIR* value just above 1.0 and a relatively large μ_{MA} due to the relatively constant *MA* and *SI* functions. In contrast, a spike/earthquake pattern corresponds to a very large *SIR* and a very small μ_{MA}. For a pattern of seismic tremors, both *SIR* and μ_{MA} should have intermediate values.

[15] To pinpoint the exact ranges of *SIR* and μ_{MA} that correspond to the majority of seismic tremors, we visually examine seismic records of February and March 2003 when an ETS event was ongoing in northern Cascadia. Approximately 744 hours of waveform data from 22 stations are included in the visual analysis. Among them, 6788 station-hours are classified as having tremor patterns, 5894 station-hours as patterns of background noise, and 2477 station-hours as patterns of spikes/earthquakes. Nearly all waveforms (>99%) with typical tremor patterns have *SIR* and μ_{MA} values of 1.2–2.2 and 0.55–1.25, respectively. About 95% of waveforms showing typical patterns of background noise have $SIR < 1.1$ or $\mu_{MA} > 1.55$, whereas waveforms with $SIR > 3.0$ or $\mu_{MA} < 0.15$ always contain spiky signals (e.g., earthquakes). Figure 2 shows the logic chart of pattern classification and the

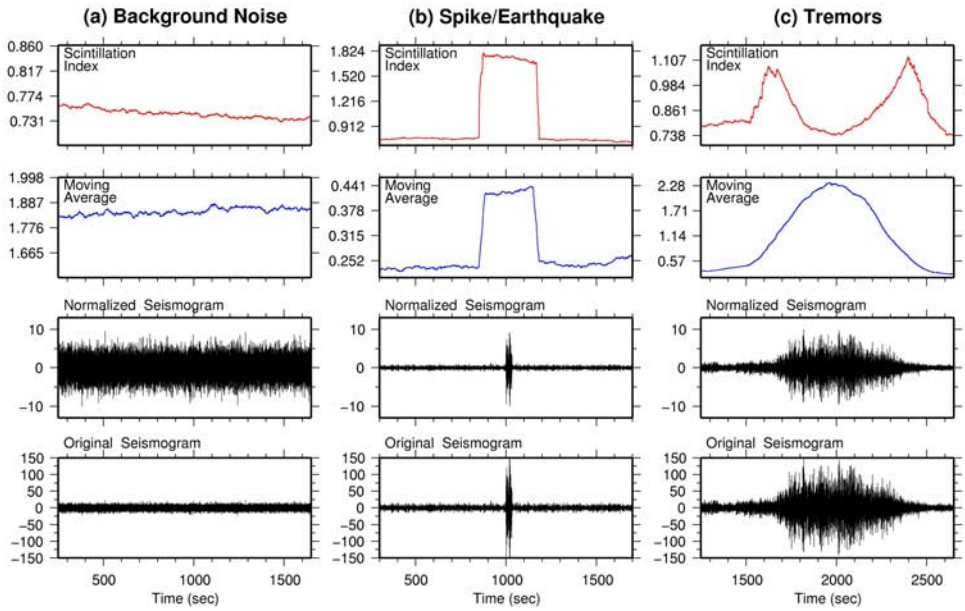

Figure 1. Scintillation index and moving average functions for the three commonly observed seismic patterns: (a) background noise, (b) spikes or earthquakes, and (c) tremors. The original and normalized waveforms (the max amplitude is set to10) are shown at the bottom. Notice that different waveform patterns exhibit significantly different values and shapes of the two functions. A window length of 300 s is used in all scintillation index and moving average calculations.

threshold of diagnostic parameters empirically determined for each pattern.

[16] While *SIR* and μ_{MA} are good indicators to characterize the three typical patterns, we need to introduce additional parameters to help identifying the less typical ones, (i.e., those with intermediate values of *SIR* and μ_{MA}, Figure 2 (right)). After trying numerous combinations, our experiments indicate that the standard deviation of the *MA* function (σ_{MA}) is particularly useful in differentiating a relatively "weak" tremor patterns from the patterns of background noise, whereas the ratio between the standard deviation and the mean of the *SI* function (σ_{SI}/μ_{SI}) is suitable for recognizing the difference between waveforms containing a small local earthquake and those with relatively "sparse" tremor bursts. An extensive collection of waveform examples and their corresponding *SI* and *MA* functions is given in the supplement to fully demonstrate the various waveform characteristics associated with each logic box in Figure 2.

[17] Once a waveform is recognized as having a tremor pattern, the approximate arrival times of tremor bursts are estimated and compared to those found in nearby stations

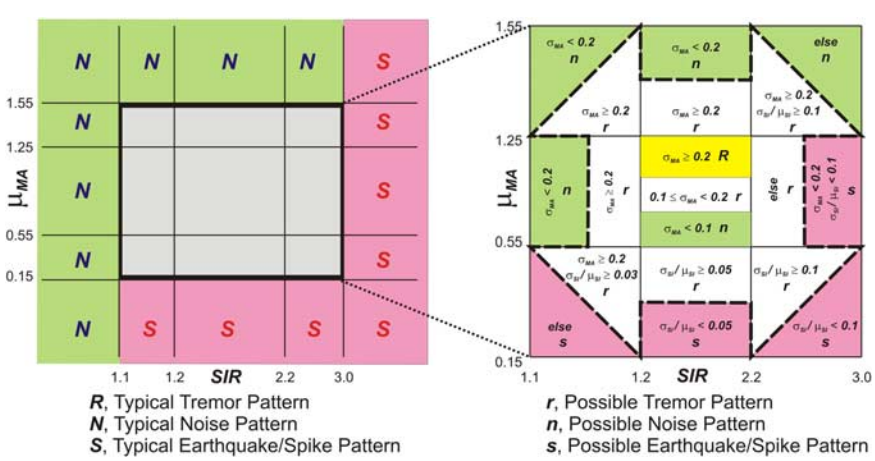

Figure 2. Logic chart for pattern characterization of seismic waveforms recorded in northern Cascadia. (left) The scintillation index ratio (*SIR*) and mean of the moving average function (μ_{MA}), both defined in the text, are used to identify waveforms showing typical patterns of background noise (marked by *N*) and earthquakes (marked by *S*). (right) Waveforms with intermediate *SIR* and μ_{MA} values are further classified. A typical tremor pattern is characterized by *SIR* of 1.2–2.2 and μ_{MA} of 0.55–1.25 with a relatively large standard deviation of the moving average function ($\sigma_{MA} \geq 0.2$).

A-4

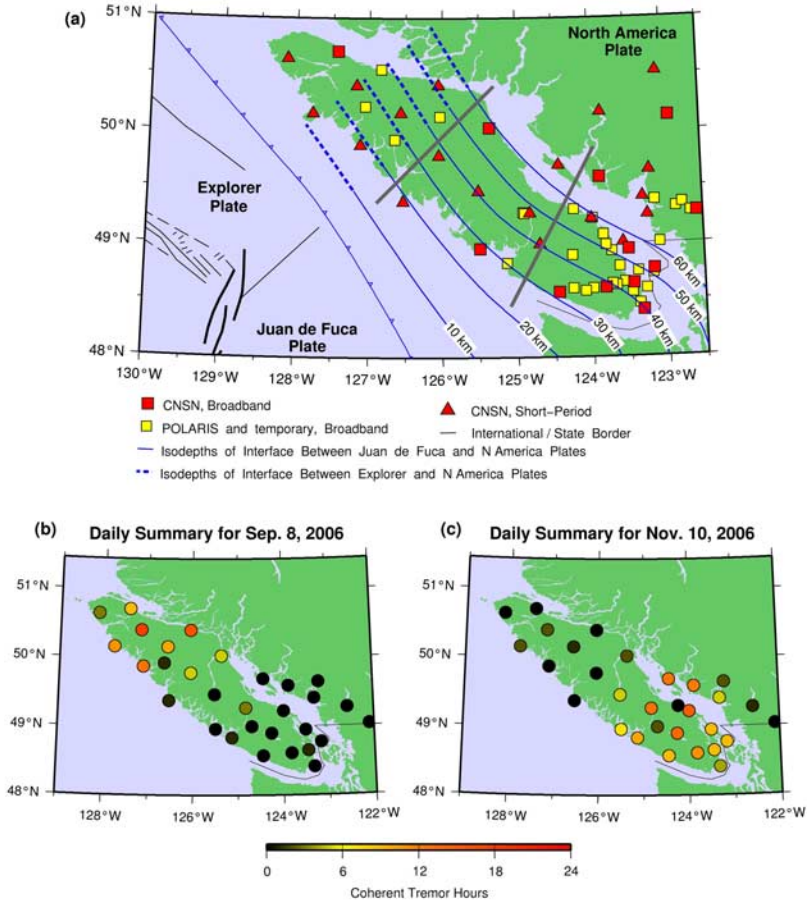

Figure 3. Classification of seismic waveform patterns for two selected days in 2006. (a) Map showing the general tectonic setting of the northern Cascadia region. Blue lines represent the surface projection of the plate interface. Available seismic stations from both permanent and temporary deployments are shown as squares (broadband) and triangles (short-period). The region is divided into three sub-regions: southern, middle, and northern, as marked by gray lines. (b) Classification summary for September 8, 2006. The number of hours showing coherent tremor patterns (*CT*) is displayed in color, as indicated by the color scale near the bottom. Notice that *CT* patterns were observed only by stations in the north. (c) Classification summary for November 10, 2006. This time, tremor activities were mainly distributed in the middle and southern sub-regions.

(in our case, within a radius of 100 km). If three or more nearby stations appear to have tremor bursts arriving at approximately the same time (a time difference <40 s), the pattern is reclassified to "coherent tremors" (*CT*). The last step is especially important in distinguishing tremors that are associated with the same ETS event from those due to natural (such as wind storm) and/or cultural/artificial sources.

4. Application to Cascadia Seismic Records of 2004–2006

[18] To further improve the proposed system, we apply it to seismic archives recorded by stations in northern Cascadia between 2004 and 2006. Specifically, we use this large dataset to fine-tune the diagnostic parameters in several logic boxes of Figure 2 that do not have sufficient number of waveform examples from the February/March 2003 ETS episode. Figure 3a shows the corresponding station distribution, including both permanent networks and temporary deployments. In Figure 3b and Figure 3c, we present the classification summaries for two selected days in 2006. On September 8, 2006, the number of hours showing *CT* patterns increases dramatically for almost all stations in the north. In contrast, nearly all stations in the southern half of Vancouver Island (VI) had prolonged *CT* hours on November 10, 2006. Not surprisingly, visual inspection of seismic and GPS data later confirmed the occurrence of ETS events in northern and southern VI during the two particular time periods, respectively.

[19] In Figure 4, we compare the classification results that are automatically generated by the proposed system to that by human visual inspection. The entire VI is divided into three sub-regions with roughly the same length to better reveal the spatial differences among different ETS episodes (Figure 3a). A "tremor hour" in the visual inspection results is counted when prominent tremor bursts can be visually recognized and correlated at more than three nearby stations. For the automatic classification results, the daily percentage of *CT* patterns found in each sub-region is plotted. The boundary between the middle and southern

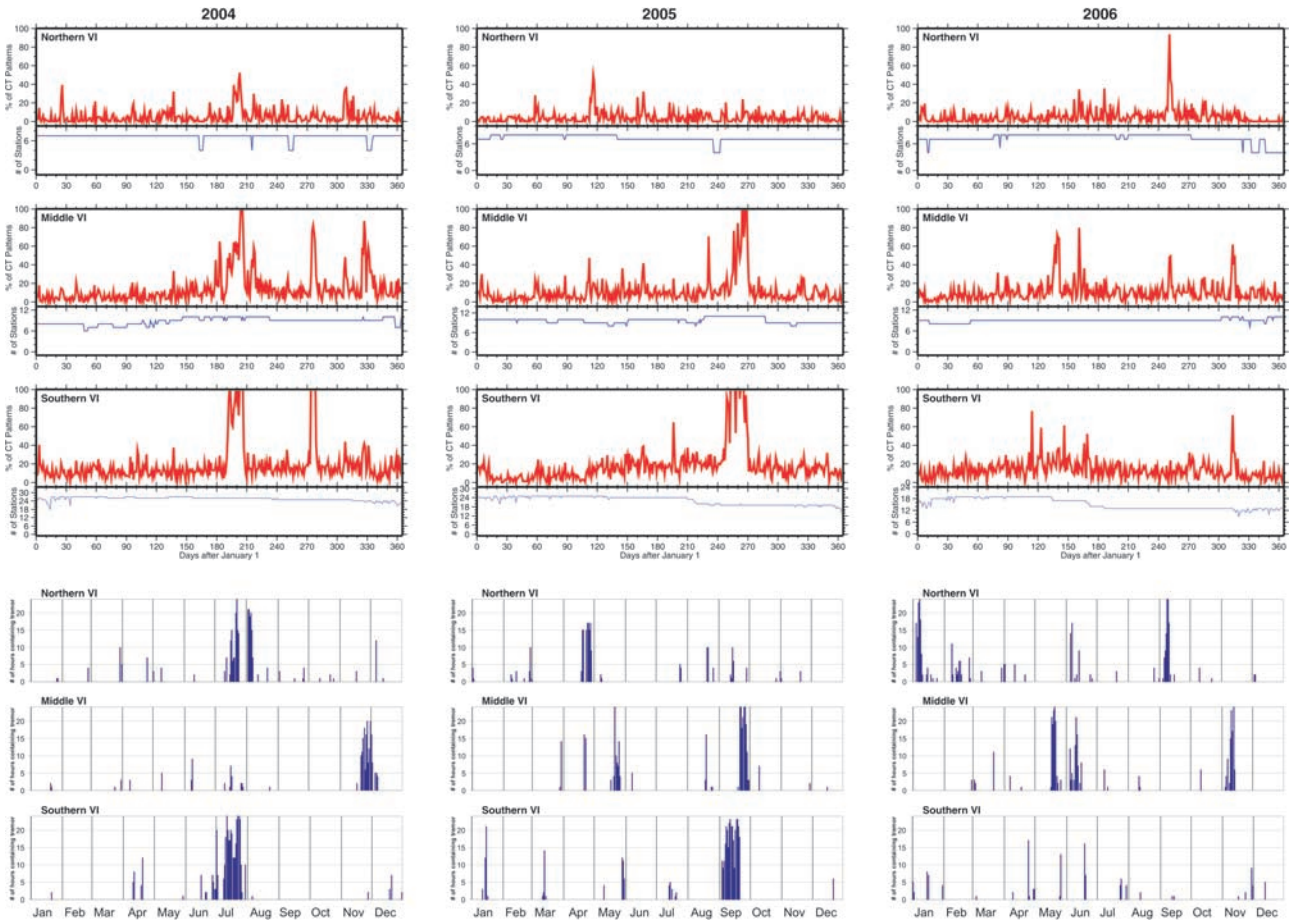

Figure 4. A comparison of the level of tremor activities (top) by the method proposed in this study and (bottom) by visual inspection. The region is roughly divided into three sub-regions: northern, middle, and southern Vancouver Island (VI), as indicated in Figure 3a. For each sub-region, the daily percentage of station-hours showing the coherent tremor (*CT*) pattern is marked by a thick red line and the number of seismic stations available for automatic classification is shown by a blue line. The corresponding number of hours containing tremor signals, as determined by visual inspection of seismograms, is shown by a blue bar below. The two approaches produce consistent results not only for major ETS episodes but also for many minor ones.

sub-regions used in the automatic classification is about 30 km to the south of the boundary used in visual inspection to ensure that the middle sub-region has enough stations to scan for coherent tremors.

[20] The overall trend of the two results agrees remarkably well with an average correlation coefficient of 0.70. The average correlation coefficient increases slightly (to 0.75) if a threshold is set to only count days with significant tremor activities. Both approaches recognize not only major ETS episodes but also numerous minor ones. Nonetheless, there are a few occasions of apparent inconsistency. Taking the middle VI in late July 2004 for example, prolonged *CT* hours were reported by the automatic system but not by visual inspection (Figure 4). It turns out that most of the differences are artifacts when tremor clusters occur in the immediate vicinity of region boundaries (which differ slightly for the two approaches).

[21] Although a comprehensive geophysical interpretation for the observed tremor pattern is beyond the focus of this paper, one important insight can be drawn from the automatic classification results in Figure 4. Specifically, the recurrence interval of major ETS events in southern VI is remarkably regular at 14 months, whereas the interval in the north is significantly shorter (about 9 months). Since there is a big difference in the plate age and convergence rate between the north and south, our observation seems to suggest that ETS recurrences may be related to tectonic parameters.

5. Discussion and Conclusion

[22] We expect the pattern classification scheme shown in Figure 2 to work properly for regions with similar S/N conditions because all waveforms are normalized during the data processing. Networks with significantly higher or lower S/N ratios may require visual analysis of a waveform subset of various patterns to adjust the diagnostic parameters.

[23] The automatic detection of tremors depends on not only the classified patterns but also the approximate arrival times of tremor bursts (i.e., *CT* patterns). Thus, it may be necessary to empirically adjust the criteria of *CT* patterns when the proposed system is applied to seismic networks

with different station configurations. For examples, a sparse array may require a larger searching radius for coherent tremor arrivals (100 km in our case, Figure 3), whereas the minimum number of stations showing coherent tremor arrivals (3 in our case) may need to be increased if seismic data from a dense array are used.

[24] In case when tremor bursts are recorded by a sparse seismic network such that the observed waveforms are not highly correlated at multiple stations, our two-step approach is expected to work better than the methods based on cross correlation of waveform envelopes. This advantage may be particularly suitable for automatic detection and monitoring of tremor activities in regions without dense seismic arrays.

[25] Finally, given that the possibility of a megathrust earthquake in northern Cascadia increases during an ETS event [*Mazzotti and Adams*, 2004], identifying seismic tremors during the early stage of an ETS event can be highly desirable. Because the proposed system relies totally on seismic waveform records, it is capable of producing classification results in near-real-time if coupled with data acquisition of local seismic networks. The system can also be used to trigger several subsequent processes that automatically determine the preliminary locations of tremors, inform scientists involved in ETS studies, and perhaps send alerts to emergency planning agencies to raise the awareness for a possible disastrous earthquake in the immediate future.

[26] **Acknowledgments.** Constructive comments by J. Vidale and an anonymous reviewer improve an earlier version of this paper. We benefit from discussion with R. Baldwin, H. Hirose, R. Hyndman, and K. Wang. POLARIS consortium kindly provides data from the BC POLARIS array. SAC and GMT are used in data processing and generating figures. This work is supported in part by USGS NEHRP grant 06HQGR0151 (Dragert et al.) and by NSERC Discovery grants 156159-06/7 (Spence). GSC contribution 20070182.

References

Broan, K. M., et al. (2003), Transient fluid pulsing and noise in the Costa Rican subduction zone: Nearly silent slip events?, *Eos Trans. AGU*, *84*, Fall Meet. Suppl., Abstract T41E-06.

Brown, K. M., et al. (2005), Correlated transient fluid pulsing and seismic tremor in the Costa Rica subduction zone, *Earth Planet. Sci. Lett.*, *238*, 189 203.

Douglas, A., J. Beavan, L. Wallace, and J. Townend (2005), Slow slip on the northern Hikurangi subduction interface, New Zealand, *Geophys. Res. Lett.*, *32*, L16305, doi:10.1029/2005GL023607.

Gallego, A., R. M. Russo, D. Comte, V. I. Mocanu, and R. E. Murdie (2006), Non-volcanic seismic tremor in the Chile triple junction region, *Eos Trans. AGU*, *87*, Fall Meet. Suppl., Abstract T54A-02.

Kao, H., S.-J. Shan, H. Dragert, G. Rogers, J. F. Cassidy, K. Wang, T. S. James, and K. Ramachandran (2006), Spatial-temporal patterns of seismic tremors in northern Cascadia, *J. Geophys. Res.*, *111*, B03309, doi:10.1029/2005JB003727.

Mazzotti, S., and J. Adams (2004), Variability of near-term probability for the next great earthquake on the Cascadia subduction zone, *Bull. Seismol. Soc. Am.*, *94*, 1954 1959.

McCausland, W., S. Malone, and D. Johnson (2005), Temporal and spatial occurrence of deep non-volcanic tremor: From Washington to northern California, *Geophys. Res. Lett.*, *32*, L24311, doi:10.1029/2005GL024349.

Melbourne, T. I., W. M. Szeliga, M. M. Miller, and V. M. Santillan (2005), Extent and duration of the 2003 Cascadia slow earthquake, *Geophys. Res. Lett.*, *32*, L04301, doi:10.1029/2004GL021790.

Nadeau, R. M., and D. Dolenc (2005), Nonvolcanic tremors deep beneath the San Andreas Fault, *Science*, *307*, 389,doi:10.1126/science.1107142.

Obara, K. (2002a), Hi-net: High sensitivity seismograph network, Japan, *Lect. Notes Earth Sci.*, *98*, 79 87.

Obara, K. (2002b), Nonvolcanic deep tremor associated with subduction in southwest Japan, *Science*, *296*, 1679 1681.

Obara, K., and H. Hirose (2006), Non-volcanic deep low-frequency tremors accompanying slow slips in the southwest Japan subduction zone, *Tectonophysics*, *417*, 33 51.

Peterson, C., D. Christensen, S. McNutt, and J. Freymueller (2006), Non-volcanic tremor in the Alaska/Aleutian subduction zone and its relation to slow-slip events, *Eos Trans. AGU*, *87*, Fall Meet. Suppl., Abstract T41A-1550.

Rogers, G., and H. Dragert (2003), Episodic tremor and slip on the Cascadia subduction zone: The chatter of silent slip, *Science*, *300*, 1942 1943.

Seno, T., and T. Yamasaki (2003), Low-frequency tremors, intraslab and interplate earthquakes in Southwest Japan from a viewpoint of slab dehydration, *Geophys. Res. Lett.*, *30*(22), 2171, doi:10.1029/2003GL018349.

Szeliga, W., T. I. Melbourne, M. M. Miller, and V. M. Santillan (2004), Southern Cascadia episodic slow earthquakes, *Geophys. Res. Lett.*, *31*, L16602, doi:10.1029/2004GL020824.

Wallace, L. M., and J. Beavan (2006), A large slow slip event on the central Hikurangi subduction interface beneath the Manawatu region, North Island, New Zealand, *Geophys. Res. Lett.*, *33*, L11301, doi:10.1029/2006GL026009.

Yeh, K., and C.-H. Liu (1982), Radio wave scintillations in the ionosphere, *Proc. IEEE*, *70*, 324 360.

H. Dragert, H. Kao, and G. Rogers, Geological Survey of Canada, Pacific Geoscience Centre, Sidney, British Columbia V8L 4B2, Canada. (hkao@nrcan.gc.ca)

G. Spence and P. J. Thompson, School of Earth and Ocean Sciences, University of Victoria, Victoria, British Columbia V8W 2Y2, Canada.